J. Fluid Mech. (1988), *vol.* 192, *pp.* 365–391
Printed in Great Britain

Minimum-dissipation transport enhancement by flow destabilization: Reynolds' analogy revisited

By GEORGE E. KARNIADAKIS, BORA B. MIKIC AND ANTHONY T. PATERA†

Department of Mechanical Engineering, Massachusetts Institute of Technology, Cambridge, MA 02139, USA

(Received 13 May 1987)

A classical transport enhancement problem is concerned with increasing the heat transfer in a system while minimizing penalties associated with shear stress, pressure drop, and viscous dissipation. It is shown by Reynolds' analogy that viscous dissipation in a wide class of flows scales linearly with the Nusselt number and quadratically with the Reynolds number. It thus follows that transport enhancement optimization is equivalent to a problem in hydrodynamic stability theory; a more unstable flow will achieve the same Nusselt number at a lower Reynolds number, and therefore at a fraction of the dissipative cost. This transport-stability theory is illustrated in a numerical study of supercritical (unsteady) two-dimensional flow in an eddy-promoter channel comprising a plane channel with an infinite periodic array of cylindrical obstructions.

It is shown that the addition of small cylinders to a plane channel results in stability modes that are little changed in form or frequency from plane-channel Tollmien–Schlichting waves. However, eddy-promoter flows are dramatically less stable than their plane-channel counterparts owing to cylinder-induced shear-layer instability (with critical Reynolds numbers on the order of hundreds rather than thousands), and thus these flows yield heat transfer rates commensurate with those of a plane-channel turbulent flow but at much lower Reynolds number. Small-cylinder supercritical eddy-promoter flows are shown to roughly preserve the convective–diffusive Reynolds analogy, and it thus follows from the transport-stability theory that eddy-promoter flows achieve the same heat transfer rates as plane-channel turbulent flows while incurring significantly less dissipation.

1. Introduction

An essential step in a large number of industrial processes is the removal of heat from a wall to a flowing fluid stream. In many of these engineering applications it is heat exchange mechanisms that limit the performance of the overall system, and thus considerable effort has been devoted to increasing heat transfer rates by effecting transport enhancement devices or techniques (Bergles & Webb 1985). Transport-enhancement schemes can take a variety of forms, from the 'passive' addition of flow obstacles, to the 'active' modulation of the driving flow rate.

Although it is clear that large transfer coefficients can be obtained by (say) flow–obstacle-induced mixing, it is important to consider not only the desired increase in heat transfer due to this flow modification, but also the undesired increase

† To whom all correspondence should be addressed at Rm. 3-264, M.I.T., 77 Mass. Ave., Cambridge, MA 02139, USA.

in momentum transport as measured by shear stress, pressure drop, and viscous dissipation. The latter are directly reflected in tangibles such as structural integrity and pumping power, and thus must be factored into any rational approach to the transport enhancement problem. Although it is certainly well recognized that the central issue in convective transport is 'thermal-hydraulic' balance, there do not appear to be at present any general guidelines allowing for *a priori* evaluation of the hydraulic viability of a particular transport augmentation scheme.

A common form of transport enhancement is flow obstruction by cylindrical eddy promoters placed in a regular periodic fashion in a channel or pipe. An analysis of such a system for mass transfer in a channel is given by Isaacson & Sonin (1976), in which minimization of a dissipation cost function is carried out subject to an experimentally determined friction factor–Sherwood number relationship. The results of this study implicate *low-Reynolds-number* configurations as producing minimum dissipation for a given mass transfer rate.

This study of mass transfer in an eddy-promoter channel system raises the general question of the relative merit of high-flow-rate turbulent transport as compared to low-Reynolds-number unsteady or transitional transport. Even more generally, it is of interest to determine if simple hydrodynamic arguments can be put forth that isolate the critical phenomena or parameters that determine the relationship between 'desirable' heat or mass transfer and 'unwanted' viscous dissipation. In this paper we show that to a first, admittedly rough, approximation, a general statement relating transport and dissipation can be made.

Our point of departure, not surprisingly, is the classical Reynolds analogy, which relates momentum transfer and heat transfer in flows dominated by a convective–diffusive balance (Reynolds 1874). The Reynolds analogy is, somewhat anomalously, exact for the case of the laminar flat-plate boundary layer at unity Prandtl number (Schlichting 1968); however, attempts to find other non-trivial instances in which the analogy is rigorous have failed (Magen, Mikic & Patera 1988). Nevertheless, in flows in which direct pressure effects are small, in which a strong convective–diffusive balance prevails, and in which the gradients in velocity and temperature appear in similar ways in their respective equations, the Reynolds analogy does appear to be valid.

Taking the Reynolds analogy as given, it then follows from simple momentum and energy integrals that shear stress, pressure drop, and viscous dissipation are all reduced if a lower-Reynolds-number flow can be found that achieves the same heat transfer rate as a higher-Reynolds-number flow. This, in turn, implies that the problem of design of optimal heat-transfer enhancement systems is best considered as a problem in hydrodynamic stability theory; a more unstable flow (that is, a flow with a lower critical Reynolds number) will generate larger Reynolds fluxes at lower Reynolds numbers, and thus achieve commensurate heat transfer at a fraction of the dissipative penalty.

In this paper we demonstrate the validity of this dissipation-transport stability theory for the problem of unsteady moderate Reynolds number two-dimensional flow in a channel disrupted by a periodic array of cylindrical eddy promotors. In §2 the governing equations are presented, and the spectral-element numerical methods used to solve the Navier–Stokes and energy equations are briefly described. In §3 the heat-transfer enhancement problem is posed, and the Reynolds analogy is evoked to reduce the optimization study to an equivalent problem in hydrodynamic stability theory. In §4, the stability of eddy-promoter channel flows is described, and related to the classical theory for plane Poiseuille flow. Lastly, in §5, results are presented

for dissipation and transport in eddy-promoter systems. Reynolds' analogy is shown to hold in the laminar unsteady flows studied, and the stability-transport arguments and associated implications are demonstrated to be valid.

The main thrust of the current paper is the study of the oft-quoted but rarely quantified relationship between transport enhancement and flow stability. Thus, our treatment of the stability of eddy-promotor flows is primarily limited to those concepts directly related to transport and dissipation. A future paper (G. E. Karniadakis, H. Kozlu, & A. T. Patera, in preparation) will describe the stability of eddy-promoter flows in greater depth.

2. Governing equations

2.1. *The nonlinear problem*

The geometry to be considered is the periodic eddy-promoter channel shown in figure 1, consisting of a planar channel disrupted by a regular periodic array of cylindrical obstacles. The channel is infinite in extent in the streamwise (x) and spanwise (z) directions, and the flow is therefore assumed to be fully developed in x and independent of z. The thermal boundary conditions are taken to be that of uniform flux on the bottom wall, ∂D_{B}, with an adiabatic top surface, ∂D_{T}, and adiabatic cylinder surfaces, ∂D_{C}. Natural convection, variation of thermal properties, and non-fully developed effects are all assumed to be negligible. The problem statement that follows is similar to that of our previous studies on periodically grooved channels (Ghaddar *et al.* 1986*b*, *c*).

To put the problem in non-dimensional form we scale all velocities by $\frac{3}{2}V$, where V is the cross-channel average velocity

$$V = (2h)^{-1} \int_{\partial D_{\mathrm{B}}}^{\partial D_{\mathrm{T}}} u(x, y, t)\, \mathrm{d}y,$$

and u is the streamwise (x) velocity. Length is non-dimensionalized by the channel half-width h, and temperature by $q''h/k$, where q'' is the uniform flux imposed at the bottom wall, ∂D_{B}, and k is the thermal conductivity of the fluid. (Hereinafter all variables are assumed to be non-dimensional unless otherwise indicated.) This gives the following equations for the velocity, $\boldsymbol{v}(\boldsymbol{x}, t)$ $(= u\hat{\boldsymbol{x}} + v\hat{\boldsymbol{y}})$, and the temperature, $T(\boldsymbol{x}, t)$:

$$\boldsymbol{v}_t = \boldsymbol{v} \times \boldsymbol{\omega} - \boldsymbol{\nabla}\Pi + R^{-1}\nabla^2\boldsymbol{v} \quad \text{in } D, \tag{1a}$$

$$\boldsymbol{\nabla}\cdot\boldsymbol{v} = 0 \quad \text{in } D, \tag{1b}$$

and

$$T_t + \boldsymbol{\nabla}\cdot(\boldsymbol{v}T) = (R\,Pr)^{-1}\nabla^2 T \quad \text{in } D, \tag{2}$$

respectively, where the domain D is defined by the channel half-width h, the periodicity length between cylinders L, the diameter of the cylinders d, and the vertical cylinder placement b. Here Π is the total pressure, $\Pi = p + \frac{1}{2}|\boldsymbol{v}|^2$; $\boldsymbol{\omega}$ is the vorticity, $\boldsymbol{\omega} = \boldsymbol{\nabla} \times \boldsymbol{v}$; $R = \frac{3}{2}Vh/\nu$ is the Reynolds number; and $Pr = \nu/\alpha$ is the Prandtl number. Also, ν and α are the kinematic viscosity and thermal diffusivity, respectively, and $\nu = \mu/\rho$, where μ is the dynamic viscosity and ρ is the density.

The fully developed boundary conditions for the velocity $\boldsymbol{v}(\boldsymbol{x}, t)$ are

$$\boldsymbol{v}(\boldsymbol{x}, t) = 0, \quad \text{on } \partial D, \tag{3a}$$

$$\boldsymbol{v}(x + mL, y, t) = \boldsymbol{v}(x, y, t), \tag{3b}$$

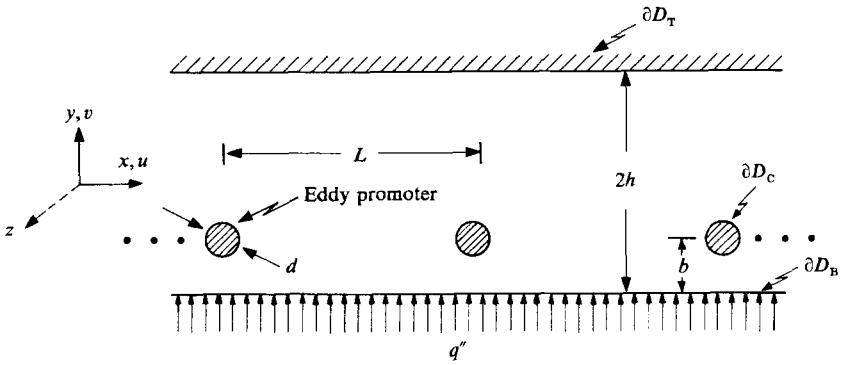

FIGURE 1. The geometry of the periodic eddy-promoter channel is described by the distance between the eddy-promoter cylinders, L, the diameter of the eddy promoters, d, and the distance of the eddy promoters from the bottom wall, b. The geometry is assumed infinite in the streamwise (x) and spanwise (z) directions.

where m is an integer periodicity index. For the pressure we require

$$\Pi(\boldsymbol{x}, t) = -f(t)\, x + \tilde{\Pi}(\boldsymbol{x}, t), \tag{4a}$$

$$\tilde{\Pi}(x + mL, y, t) = \tilde{\Pi}(x, y, t), \tag{4b}$$

where $f(t)$ is the driving force for the flow, and is determined indirectly by the imposed flow-rate condition

$$Q = \int_{\partial D_B}^{\partial D_T} u(x, y, t)\, \mathrm{d}y = \tfrac{4}{3}. \tag{5}$$

For the temperature boundary conditions on the channel and cylinder walls we have

$$\nabla T \cdot \hat{\boldsymbol{n}} = 1 \quad \text{on } \partial D_B, \tag{6a}$$

$$\nabla T \cdot \hat{\boldsymbol{n}} = 0 \quad \text{on } \partial D_T \cup \partial D_C, \tag{6b}$$

respectively, where $\hat{\boldsymbol{n}}$ refers to the outward normal on the domain boundary. As discussed in previous work on periodic-groove flows (Patankar, Liu & Sparrow 1977; Ghaddar *et al.* 1986*c*; Ghaddar, Karniadakis & Patera 1986*a*), the correct fully developed periodic boundary condition on $T(\boldsymbol{x}, t)$ is

$$T(\boldsymbol{x}, t) = \theta(\boldsymbol{x}, t) + \frac{\frac{3}{4}x}{RPr}, \tag{7a}$$

$$\theta(x + mL, y, t) = \theta(x, y, t), \tag{7b}$$

where the linear-in-x temperature term must be included to balance the heat input at the bottom channel wall (6*a*).

It should be noted that, although we shall ultimately be interested in the relationship between viscous dissipation and heat transport, all coupling between the fluid and heat transfer equations is via the convective terms in (2). In particular, the temperature is passive, and does not drive the fluid flow, and the viscous dissipation does not enter as a source in the energy equation.

2.2. *The linear stability problem*

In addition to the full nonlinear problem described by (1) and (3)–(5) it will also be of interest to consider the linearized problem about a steady solution to the Navier–Stokes equations, $\boldsymbol{v}_s(\boldsymbol{x})$, in which we assume solutions of the form

$$\boldsymbol{v}(\boldsymbol{x},t) = \boldsymbol{v}_s(\boldsymbol{x}) + \epsilon \boldsymbol{v}'(\boldsymbol{x},t), \quad \epsilon \ll 1. \tag{8}$$

Inserting (8) into (1) and neglecting terms $O(\epsilon^2)$ and higher gives the following linear equation for $\boldsymbol{v}'(\boldsymbol{x},t)$:

$$\boldsymbol{v}'_t = \boldsymbol{v}_s \times \boldsymbol{\omega}' + \boldsymbol{v}' \times \boldsymbol{\omega}_s - \nabla \Pi' + R^{-1} \nabla^2 \boldsymbol{v}' \tag{9a}$$

$$\nabla \cdot \boldsymbol{v}' = 0. \tag{9b}$$

The boundary conditions on the perturbations $\boldsymbol{v}'$, Π' are as in (3)–(4), but the flow-rate condition (5) is now replaced with

$$Q' = \int_{\partial D_B}^{\partial D_T} u'(x,y,t)\, \mathrm{d}y = 0, \tag{10}$$

corresponding to no net perturbation flow.

For sufficiently large times, the solution of the initial-value problem (9)–(10) will approach the least stable mode of the eigenvalue problem resulting from normal-mode formulation of the same equation. In particular, the initial-value-problem result can be interpreted as

$$\boldsymbol{v}'(\boldsymbol{x},t) \sim \exp(\sigma t)\, \mathrm{Re}\{\hat{\boldsymbol{v}}'(\boldsymbol{x}) \exp(2\pi \mathrm{i} \Omega t)\} \quad (t \to \infty), \tag{11}$$

from which the growth rate σ, and frequency Ω, of the most unstable mode can be deduced. It should be noted that the time-asymptotic behaviour of (9)–(10) can be used to infer information about only the least-stable mode of the system.

2.3. *Numerical methods*

The direct numerical simulation approach followed in this investigation is very similar to that used in our grooved-channel studies (Ghaddar *et al.* 1986*b*, *c*), and we therefore only briefly summarize our methods. The basic philosophy is to use initial-value-problem solvers in all aspects of the work; steady states, their linear stability, and subsequent nonlinear oscillations and transport are all determined using essentially the same initial-value code, with only the interpretation of the results depending on the particular physical phenomenon of interest. The governing partial differential equations (1)–(7) are solved using finite differences in time and the isoparametric spectral-element method in space. The spectral-element method (Patera 1984; Korczak & Patera 1986; Ghaddar *et al.* 1986*a*) is a high-order weighted-residual technique that combines the geometric flexibility of finite-element schemes (Girault & Raviart 1986) with the rapid convergence rate, good resolution properties, and minimal dispersion of global spectral methods (Gottlieb & Orszag 1977).

In the spectral-element discretization the computational domain is broken up into macro-spectral elements, and the dependent and independent variables are approximated by Nth-order tensor-product polynomial expansions within the individual subdomains. Variational projection operators and Gauss numerical quadrature are used to generate the discrete equations, which are then solved by direct or iterative procedures using tensor-product sum-factorization techniques. Convergence to the exact solution is achieved by increasing the degree N of the

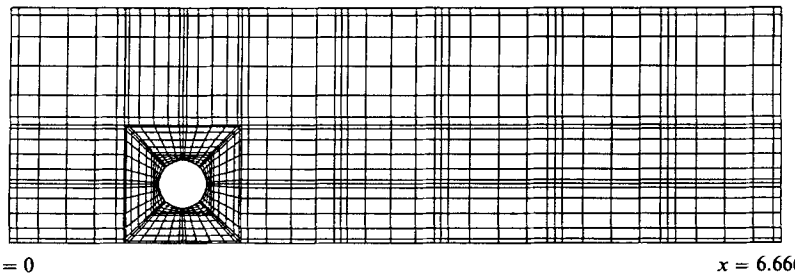

FIGURE 2. Spectral-element mesh for the base-geometry eddy-promoter geometry, $L = 6.666$, $d = 0.4$, $b = 0.5$. Fine resolution is placed near the cylinder surface to ensure accurate representation of the thin boundary layers and wake structures expected to form near the eddy promoters. The cylinder is placed (arbitrarily) at $x = 1.50$.

polynomial approximation, while keeping fixed the number and identity of the underlying spectral elements. Although results presented in this paper are based primarily on time-splitting Stokes solvers and Chebyshev interpolants in space, current work uses improved schemes based on non-splitting Stokes algorithms and Legendre interpolants in space (Rønquist & Patera 1987; Maday & Patera 1988).

A typical calculation of an eddy-promoter flow at a Reynolds number of $R = 225$ is carried out on a mesh such as that shown in figure 2, with 1400 (global) nodes and a timestep of $\Delta t = 0.005$. To resolve one period of the unsteady flow requires 1000 timesteps, and an execution time of roughly 2.5 min (per period) on a single-headed CRAY X-MP. All numerical calculations presented in this paper have been determined to be sufficiently mesh- and timestep-independent to be considered accurate solutions of the unsteady Navier–Stokes and energy equations; this is verified by comparison of solutions on different meshes, as well as by inspection of global momentum and energy balances. The code employed in the current study has been used in many past investigations in which exhaustive comparisons with experiment and theory have been performed, one germane example of which is the accurate propagation of Tollmien–Schlichting waves shown in figure 4 of Ghaddar *et al.* (1986*b*).

Lastly, we note that the spectral-element results of this paper agree well with a set of companion experiments in water and wind tunnels (Kozlu, Mikic & Patera 1988; H. Kozlu, research in progress for a Ph.D. thesis at MIT), indicating that the assumptions implicit in the problem formulation (1)–(7) (e.g. two-dimensionality, periodicity) are, indeed, a reasonable approximation to physical reality for the parameter range studied.

3. Dissipation-transport theory

3.1. *The transport enhancement problem*

The eddy-promoter channel system shown in figure 1 is representative of a wide class of engineering heat exchange problems. In most of these applications the design requirement is that the temperature on the heated wall, ∂D_{B}, remain below some prescribed level for a given imposed heat flux q''. In order to satisfy this maximum-wall-temperature requirement two approaches can be pursued: the Reynolds number of the flow can be increased while keeping the geometry fixed; or the eddy-promoter geometry can be modified while keeping the Reynolds number fixed. It is typically the case that with either one of these remedies the requisite increase in heat transfer coefficient can be obtained, and thus the distinction between the two choices

is determined solely by the optimality criteria used to evaluate the overall system performance.

Although there is no single optimality criterion that encompasses all transport applications, it is generally true that a design that reduces shear stress, pressure drop, and viscous dissipation will be a good, if not optimal, transport enhancement procedure. Shear stress and pressure drop relate to structural integrity, whereas viscous dissipation translates directly into energy consumption. We shall therefore define the 'enhancement problem' as follows: Find the optimal flow rate V and eddy-promoter configuration L, d, and b so as to minimize shear stress, pressure drop, and viscous dissipation for a given heat transfer rate per unit wall-temperature elevation.

In order to pose this problem more quantitatively we introduce non-dimensional measures of heat transfer, shear stress, pressure drop, and dissipation. The heat transfer is characterized by a Nusselt number,

$$Nu = L \Big/ \int_0^L \langle \theta - \theta_b \rangle \, \mathrm{d}x|_{\partial D_B}, \tag{12a}$$

where θ_b is a reference temperature taken to be the (periodic part of the) mixed-mean temperature at $x = 0$,

$$\theta_b = \frac{3}{4} \int_{-1}^{1} \langle u(x=0,y,t)\, \theta(x=0,y,t) \rangle \, \mathrm{d}y, \tag{12b}$$

and angle brackets indicate a time average. The Nusselt number can be thought of as a non-dimensional heat transfer coefficient, as a flux per unit temperature elevation, or as an inverse average wall temperature. It should be noted that all quantities required in (12) are readily determined experimentally.

For shear stress, pressure drop, and viscous dissipation we use the following non-dimensional parameters:

$$\tau = \tfrac{1}{2} \langle \tau_w \rangle h^2/\rho\nu^2, \tag{13a}$$

$$\pi = \frac{1}{2} \left\langle \frac{\mathrm{d}p}{\mathrm{d}x} \right\rangle h^3/\rho\nu^2, \tag{13b}$$

and

$$\Phi = \frac{3}{4} \left\langle \frac{\mathrm{d}p}{\mathrm{d}x} \right\rangle Vh^4/\rho\nu^3, \tag{13c}$$

respectively, where all quantities on the right-hand side of (13) are dimensional: τ_w is the spatially averaged shear stress over $\partial D_B \cup \partial D_T$, and $\mathrm{d}p/\mathrm{d}x$ is the dimensional form of the constant-pressure-gradient term $f(t)$ in (4). Note that the control variables of the problem, V, L, d, and b, do not enter explicitly into the non-dimensionalizations of shear stress, pressure drop, and dissipation, and thus minima of the non-dimensional parameters τ, π, and Φ will reflect true minima of the corresponding dimensional quantities of interest, τ_w, $\langle \mathrm{d}p/\mathrm{d}x \rangle$, and $\langle \mathrm{d}p/\mathrm{d}x \rangle Vh$, respectively.

Armed with the definitions given above, we can write the transport-enhancement problem as

$$\min_{R,L,d,b} \mathscr{H}(\tau, \pi, \Phi) \quad \text{for fixed } \{Nu; h; \rho, \nu, Pr, k\}, \tag{14}$$

where $\mathscr{H}(\cdot,\cdot,\cdot)$ is some cost function which is a monotonically decreasing function of all three arguments. Note that by fixing h in (14) we are essentially fixing the scale of the apparatus; extension of the analysis to include optimization with respect to channel size is given in Kozlu *et al.* (1988). In the current paper we shall not consider

the minimization of any particular $\mathscr{H}(\tau, \pi, \Phi)$, but will rather focus on understanding the fundamental unsteady hydrodynamic phenomena that relate τ, π, Φ, and Nu in complex geometry flows.

Before proceeding we shall make a point concerning the practical relevance of (14). The total (non-dimensional) temperature rise along the heated wall, δT, is actually composed of two parts (see (7*b*)), $\delta T = \delta T_q + 1/Nu$. Here δT_q is the 'thermodynamic' temperature rise due to the flux input q'', $\delta T_q = \frac{3}{4}x/RPr$, and $1/Nu$ is the 'transport-limited' temperature difference between the wall and local fluid temperature. It is clear that in the design of real cooling systems it is δT, not Nusselt number, that should be constrained. Although the fixed-δT optimization problem can be solved (Kozlu *et al.* 1988), the basic fluid-dynamical arguments that result are the same as for the fixed-Nu case, and we therefore proceed with the simpler optimization (14). It should be also noted that in many (fixed h) systems $Nu\delta T_q \ll 1$, in which case the distinction between $1/Nu$ and δT is no longer important.

3.2. *Reynolds' momentum–heat transfer analogy*

The solution or understanding of (14) depends primarily on the ability to relate the transport of momentum with the transfer of heat. The idea that momentum and heat transport are related in a fundamental and simple way is very old, dating back to the seminal work of Osborne Reynolds (1874). Indeed, Reynolds' analogy is at the heart of much current forced-convection heat-transfer research and practice (Kays & Crawford 1980).

Roughly speaking, the analogy states that in any flow in which momentum and heat transport are dominated by a strong convective–diffusive balance, in which velocity and temperature boundary conditions are similar, and in which the 'outer' flow is well mixed so as to make the wall structures universal and geometry-independent, the shear stress (momentum flux) and heat flux at the wall scale similarly. These criteria are typically met in turbulent flows, in which the Reynolds stress and Reynolds flux terms (velocity–velocity correlations and velocity–temperature correlations, respectively) are large compared with molecular diffusion through mean gradients. Although to date no rigorous theoretical work exists that proves the validity of the Reynolds analogy for general flows, certain upper-bound results have been obtained (Magen *et al.* 1988).

As an example of how the Reynolds analogy is typically applied, we take the case of channel flow without eddy promoters ($d = 0$ in figure 1). For this flow, Reynolds' analogy takes the form

$$\frac{\langle \tau_w \rangle}{\mu V/h} = \frac{\gamma q''}{k\langle \Delta T \rangle/h}, \tag{15a}$$

where all variables save γ are dimensional, and $\langle \Delta T \rangle$ represents the time–space average of the bottom-wall-to-bulk (mixed-mean) temperature difference. In terms of our non-dimensional variables (12)–(13), (15*a*) can be rewritten as

$$\tau = \tfrac{1}{3}\gamma RNu. \tag{15b}$$

The parameter γ in (15) is the 'Reynolds-analogy constant', which, if the analogy applies, is a constant close to unity for $Pr = 1$ that is independent of Reynolds number R and flow geometry. More precisely, γ should be a function only of Prandtl number.

For turbulent channel and pipe flows a wealth of experimental observations (Kays

& Crawford 1980; H. Kozlu 1988, research in progress) support (15*b*) with γ quite close to unity (i.e. to within several percent). Although the precise value of γ will depend on the particular average velocity and temperature scales chosen (V and $\langle \Delta T \rangle$, respectively, in (15)), in high-Reynolds-number turbulent flows the outer flow is well-mixed, and the value of γ should be relatively insensitive to the choice of mean variables (Taylor 1930).

For laminar channel flow the value of γ in (15) can readily be shown to be 2.22 independent of the Reynolds number. Although this value is not close to unity, this is not the real basis for rejecting the Reynolds analogy, as velocity and temperature scales could be chosen so as to achieve $\gamma = 1$. Rather, it is the fact that γ is strongly sensitive to the choice of mean scales that indicates that the analogy is not 'valid': there is no convective–diffusive balance in the purely diffusive laminar flow, and γ reflects the detailed forcing functions and boundary conditions rather than universal wall structures.

Somewhat anomalously, the one instance in which the Reynolds analogy is non-trivially exact is for a laminar flow, namely the flat-plate boundary layer at Prandtl number of unity (Schlichting 1968). The Reynolds-analogy convective–diffusive balance applies in this laminar flow owing to simple geometry and the absence of pressure terms. The fact that the analogy holds for the steady boundary layer as well as highly unsteady turbulent flows is, perhaps, not coincidental; transport to the wall in turbulent flows can be viewed at the instantaneous level as a series of boundary sublayer events, as described by surface-renewal models (Thomas 1979; Mikic 1981). The surface-renewal picture of wall structures allows the Prandtl-number dependence of γ to be inferred as $\gamma \sim Pr^{-\frac{1}{3}}$ (for Pr not small), which is in good agreement with experimental evidence (Kays & Crawford 1980).

For the purpose of understanding transport enhancement in eddy-promoter channels we require several extensions to Reynolds' analogy: its range of applicability must be extended to highly unsteady laminar flows as well as turbulent flows; the effects of 'non-analogous' components of momentum transport in a complex geometry flow must be quantified; its implications as regards dissipation must be understood. We now turn to these issues.

3.3. *Relationship between dissipation, transport, and stability*

Our ultimate interest is in understanding transport in highly unsteady moderate-Reynolds-number laminar eddy-promoter flows, that is, in eddy-promoter flows that are significantly supercritical as regards the linear stability limit. Although Reynolds' analogy is typically applied only to turbulent flows, the general criteria for its validity (e.g. Reynolds-flux-dominated transport) would appear to apply equally well to sufficiently supercritical laminar flows. In particular, the global statement (15) cannot distinguish between transport effected by low-wavenumber coherent secondary flows in ordered flows, and transport by random fluctuations and small-scale excitation in disordered flows.

We therefore assume for now that the Reynolds analogy applies in the eddy-promoter geometry for all sufficiently supercritical Reynolds numbers (laminar or turbulent), and return to this point in §5 to provide numerical verification of the claim. We can thus write, as in (15),

$$\tau = \tfrac{1}{3}\gamma RNu, \tag{16}$$

where τ is the non-dimensional average shear stress on $\partial D_{\mathrm{B}} \cup \partial D_{\mathrm{T}}$. We make two points concerning (16). First, (16) says nothing concerning momentum flux at the

cylinder surface, ∂D_C, as τ reflects only the shear stress at the two channel walls. Second, (16) implicitly assumes symmetry (in the average) for the shear stress on the two channel walls. It will be shown in §5 that the flow structures generated by the eddy-promoter cylinders are, indeed, roughly symmetric on the average.

Having established (16), it is a simple matter to apply an x-momentum balance to a periodicity interval control volume ($x < x' < x+L$) to arrive at

$$\pi = \tfrac{1}{3}\gamma\, RNu + \pi_C, \tag{17a}$$

$$\pi_C = \tfrac{1}{18} C_D \frac{d}{L}\left(\frac{V_C}{V}\right)^2 R^2, \tag{17b}$$

where C_D is the drag coefficient on the cylinder,

$$C_D = F_D / \tfrac{1}{2}\rho V_C^2\, d. \tag{18}$$

Here F_D is the dimensional drag force on a single eddy promoter cylinder, and V_C is the dimensional local velocity used to non-dimensionalize F_D, taken to be $V_C = \frac{3}{2}V(1-(1-b)^2)$. At this point we do not conjecture as to the form of C_D.

Having obtained the pressure drop π, we can now calculate the total dissipation in the flow, which is simply the flow work term arising from the non-periodic part of the pressure,

$$\Phi = \tfrac{1}{3}\gamma\, R^2 Nu + \Phi_C, \tag{19a}$$

$$\Phi_C = \tfrac{1}{18} C_D \frac{d}{L}\left(\frac{V_C}{V}\right)^2 R^3. \tag{19b}$$

The terms involving the drag on the cylinder in (17) and (19), π_C and Φ_C, respectively, represent 'non-analogous' momentum transfer, in that as the eddy promoters are specified as adiabatic, the shear stress and pressure forces on the cylinder have no thermal analogue. (The pressure forces would, of course, have no thermal analogue independent of the thermal boundary conditions applied.) It is clear that (17)–(19), and their associated implications discussed below, are generally valid for any flow involving the interaction of bluff bodies with an internal flow, and are not limited to our particular eddy-promoter system.

We are now in a position to draw a general conclusion as to which flow systems result in optimal transport enhancement according to the criteria established in §3.1. We consider two flows, I and II, which achieve a specified Nu at Reynolds numbers R_I and R_{II}, respectively. Assuming for the moment that the non-analogous cylinder drag term Φ_C is small, the ratio of the dissipations in flows I and II is given by (19a) as

$$\frac{\Phi_I}{\Phi_{II}} \sim \left(\frac{R_I}{R_{II}}\right)^2. \tag{20}$$

It follows directly that if flow I is much more unstable than flow II, that is, is able to achieve commensurate Reynolds fluxes and hence the same Nu at $R_I \ll R_{II}$, then flow I will incur significantly less dissipation than flow II. Similar arguments can be made on the basis of (16)–(17) to show that a more unstable flow also reduces pressure drop π, and shear stress τ. (By 'more unstable' in this context we mean a reduced critical Reynolds number for the primary bifurcation, although the concept of decreased stability and associated increased transport may extend to secondary instabilities and turbulent flow as well.) We note that the relationship (20) can also be interpreted as justification of the conventional heat-transfer-enhancement

wisdom, in which increases in the Nusselt number at fixed R are assumed to result in improvement in 'system performance'.

The arguments given above reduce the problem of heat transfer enhancement to an equivalent problem in hydrodynamic stability theory: Find values of L, d, and b that maximally destabilize plane-channel flow. A critical assumption in (20), however, is that the cylinder drag term Φ_C will be small compared with the 'analogous' components of the momentum transport. Indeed, it may appear paradoxical that the eddy-promoter cylinders could significantly decrease the critical Reynolds number of a channel flow, yet not contribute overly to the total drag and dissipation in the system. To understand why this is, in fact, the case, requires an investigation of the stability of eddy-promoter channel flows.

4. Stability of eddy-promoter channel flows

4.1. *Plane-Poiseuille-flow Tollmien–Schlichting waves*

For the choice $d = 0$ (no cylinders), the general problem described in §§2.1 and 2.2 reduces to that of flat-channel plane Poiseuille flow. Although this 'simple' problem may appear to be irrelevant to the problem of finite d, our results for grooved-channel flow indicate that this will not be the case (Ghaddar *et al.* 1986*b*). We therefore briefly review here the stability properties of plane Poiseuille flow (Drazin & Reid 1981).

As is well known, a solution to the plane Poiseuille flow problem is the parabolic profile, $\boldsymbol{v}_s = (1-y^2)\,\hat{\boldsymbol{x}}$. The linear stability of this flow with respect to infinitesimal disturbances of the form

$$\boldsymbol{v}'_{TS}(\boldsymbol{x}, t) = \exp(\sigma_{TS} t)\,\mathrm{Re}\{\hat{\boldsymbol{v}}'_{TS}(y)\exp(\mathrm{i}\alpha x - 2\pi\mathrm{i}\Omega_{TS} t)\} \tag{21a}$$

(Tollmien–Schlichting waves of wavelength $2\pi/\alpha$), is governed by the classical Orr–Sommerfeld equation, the least-stable mode of which we shall denote

$$\mathscr{F}(\sigma_{TS}, \Omega_{TS}, \hat{\boldsymbol{v}}'_{TS}; \alpha, R) = 0. \tag{21b}$$

Depending on the parameter values, α and R, the least-stable mode can take the form of either a wall mode (low phase speed with critical layer near the wall) or a centre mode (high phase speed with critical layer near the centre of the channel) (Drazin & Reid 1981).

Solution of (21*b*) (Orszag 1971) gives the onset of instability ($\sigma > 0$) at $R_{c,TS} = 5772$, $\alpha_{c,TS} = 1.02$. As even finite-amplitude two-dimensional disturbances to plane Poiseuille flow are stable for $R < 3000$ (Herbert 1976), we conclude that in the absence of cylinders no channel instabilities or unsteadiness would occur at the Reynolds numbers investigated in this study, $0 < R < 600$.

4.2. *Eddy-promoter channel flows*

We begin by considering subcritical and supercritical flows in the 'base' geometry, $L = 6.666$, $d = 0.4$, $b = 0.5$. Although our numerical methods are clearly not limited to any particular range of the geometric parameters, our interest is primarily in 'small' values of cylinder diameter d. Small cylinders are not only of practical interest as regards minimizing Φ_C, but are also of theoretical interest in that they allow the results to be interpreted in a perturbative sense.

The spectral-element mesh used for the calculations is shown in figure 2. Fine resolution is placed near the cylinder surface in order to resolve the thin boundary

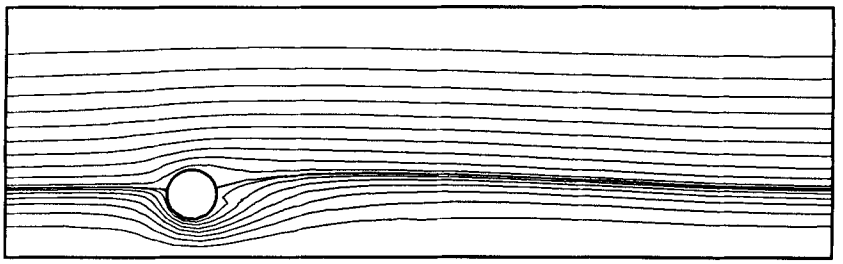

FIGURE 3. A plot of the steady streamlines in the base geometry at $R = 125$. The flow is essentially parallel with the exception of a small region corresponding to the wake of the eddy promoter.

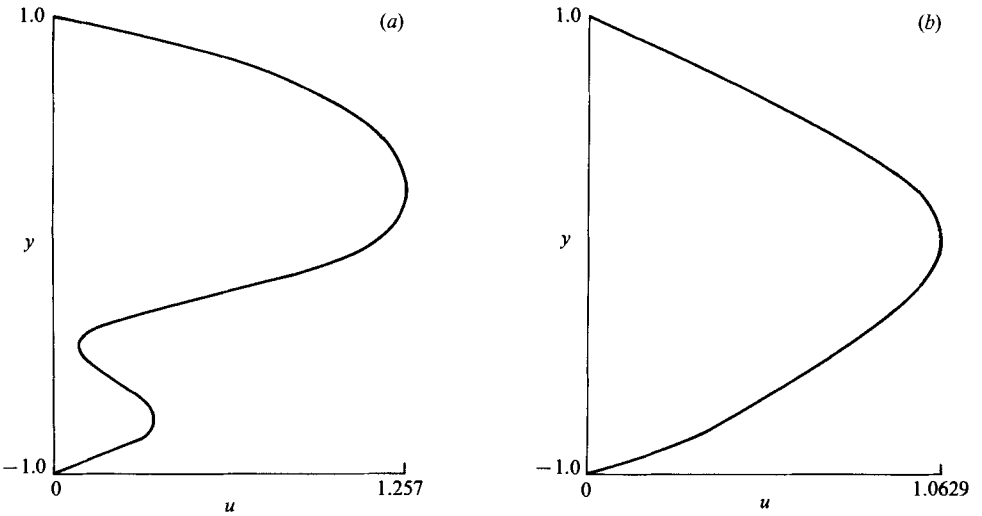

FIGURE 4. Streamwise velocity profiles of the steady flow depicted in figure 3 at (*a*) $x = 2.0$ and (*b*) $x = 6.5$ (see figure 2 for definition of streamwise (x) positions). Far from the cylinder the flow is quite close to the parabolic plane-channel result; however, in the immediate vicinity of the cylinder the geometric disturbance has a significant effect, causing the formation of local inflexion points.

layers and wake structures expected in the vicinity of the eddy promoter. In figure 3, we plot the steady streamlines obtained by integrating the spectral-element discretization of (1) to a steady state at a Reynolds number of $R = 125$. In figures 4 (*a*) and 4 (*b*) we plot streamwise velocity profiles at $x = 2.0$ and $x = 6.5$, respectively, the latter showing the (almost) parabolic profile that obtains far from the eddy promoters, the former showing the inflexional wake profiles created immediately downstream of the cylinders. In essence, the steady flow corresponds to a plane Poiseuille flow locally perturbed in the vicinity of the eddy promoters.

For this base geometry the Reynolds number of $R = 125$ results in a stable steady flow, as evidenced by the fact that the time-iterative numerical procedure converges to a steady state. To investigate the linear stability of this flow, the steady-state shown in figure 3 is used as $\boldsymbol{v}_s$ in (8)–(10), and the linearized equations are integrated in time until a time-asymptotic purified least-stable mode is obtained. Interpreting this result as described by (11) we find that the growth rate and frequency of this mode are $\sigma = -0.028$ and $\Omega = 0.185$, respectively. The unsteady streamlines of the associated eigenfunction are plotted in figure 5 at several times during the flow cycle, $0 < t < \Omega^{-1}$.

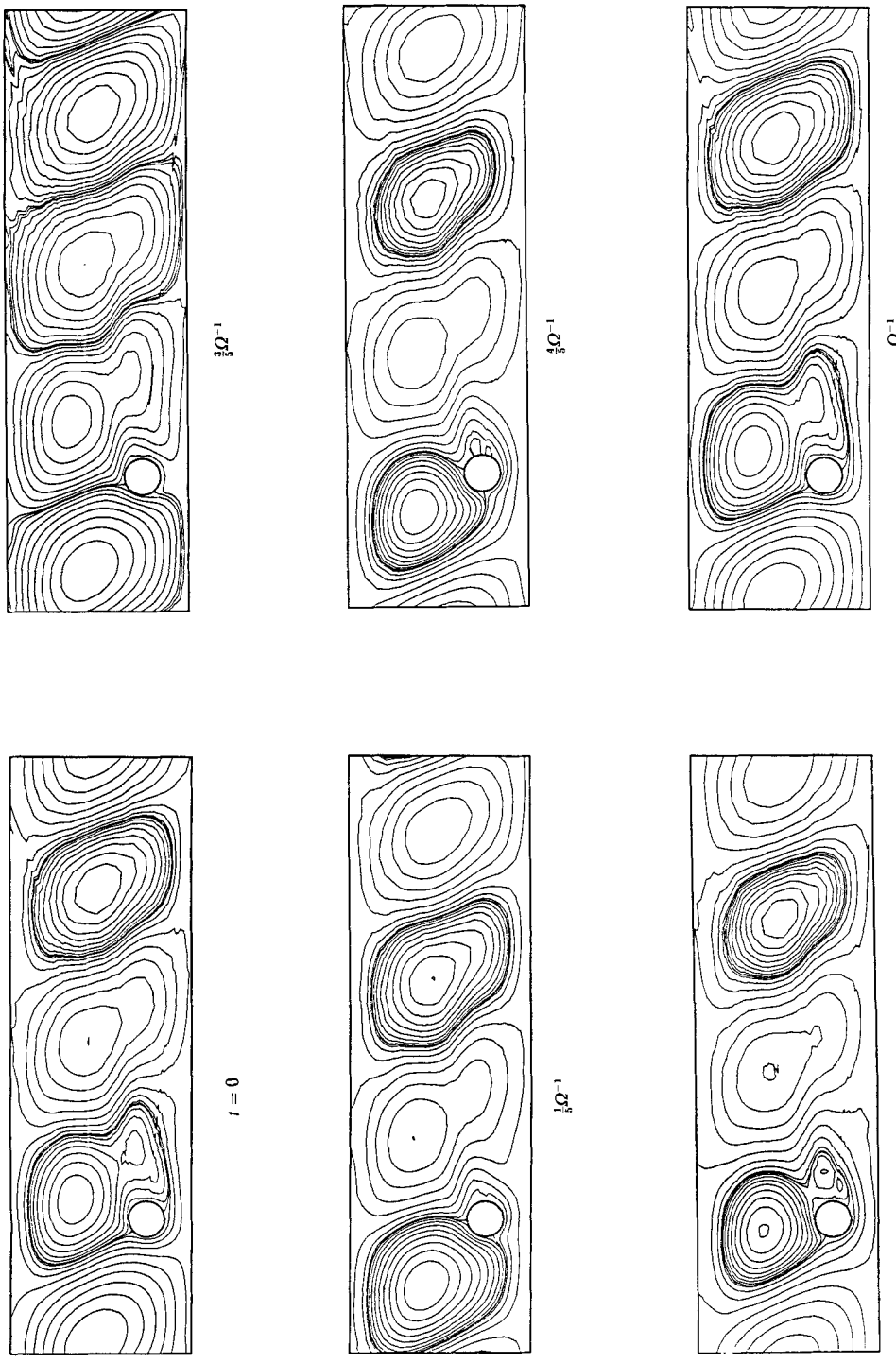

FIGURE 5. A plot of the streamlines of the least-stable (decaying) eddy-promoter channel stability mode for the base geometry at a Reynolds number of $R = 125$, at several times during the flow cycle $0 < t < \Omega^{-1}$. The stability mode is seen to be approximately a travelling wave.

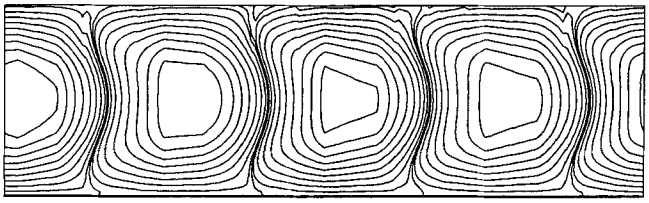

FIGURE 6. A plot of the streamlines of the least-stable plane channel ($d = 0$) Tollmien–Schlichting wave for $R = 125$, $\alpha = 1.885$. Note the similarity of this flat-channel mode with the eddy-promoter stability mode shown in figure 5.

It is clear from figure 5 that the eddy-promoter eigenfunction is approximately a travelling wave, with two wavelengths per periodicity length L. This solution is therefore denoted a two-wave solution, or $n = 2$ solution, with a wavenumber of $\alpha = (2\pi n/L) = 1.885$. Closer inspection of figure 5 reveals that the eigenfunction is not only a travelling wave, but in fact closely resembles the Tollmien–Schlichting stability waves of flat-channel ($d = 0$) plane Poiseuille flow. For comparison we plot in figure 6 the streamlines of the least-stable plane-channel Tollmien–Schlichting wave, $\boldsymbol{v}'_{\mathrm{TS}}$, for $\alpha = 1.885$, $R = 125$.

To demonstrate this similarity more quantitatively we introduce the quantity

$$s(u'; y, x) = \left(2\Omega \int_t^{t+1/\Omega} [u'(x, y, t')]^2 \, \mathrm{d}t'\right)^{\frac{1}{2}}, \tag{22}$$

where u' is the streamwise perturbation velocity. For an exact travelling wave, $s(u'; y, x)$ is precisely the modulus of the complex mode shape (e.g. $s(u'_{\mathrm{TS}}; y, x) = |\hat{u}'_{\mathrm{TS}}(y)|$), and will thus be independent of x; for the approximate-travelling-wave eddy-promoter flows $s(u'; y, x)$ will no longer be independent of x, however the functional dependence will be weak except in the immediate neighbourhood of the cylinder. In figure 7 we compare $s(u'; y, x = 6.5)$ for the eddy-promoter flow at $R = 125$ with $|\hat{u}'_{\mathrm{TS}}(y)|$ at $R = 125$, $\alpha = 1.885$. Although in the vicinity of $y = b - 1 = -0.5$ the cylinder is seen to have a significant effect on the eddy-promoter flow, in the rest of the channel the eddy-promoter and plane-channel stability modes are quite similar.

Particularly striking in figure 7 is the similarity of the critical-layer structure and position in the eddy-promoter and plane-channel stability modes. One would thus expect the two modes to have approximately the same phase speed, and hence frequency. This is, in fact, the case; the frequency of the flat-channel Tollmien–Schlichting wave is $\Omega_{\mathrm{TS}}(\alpha = 1.885, R = 125) = 0.181$, which is equal to the eddy-promoter frequency $\Omega = 0.185$ to within 2.0%. Thus, in both form and frequency, the eddy-promoter stability modes for this particular geometry are very similar to their plane-Poiseuille-flow counterparts. The similarity between the eddy-promoter and flat-channel modes does not, however, extend to stability, as might be expected from the inflexional profile shown in figure 4(*a*). Indeed, the growth rate is $\sigma = -0.028$ for the eddy-promoter channel at $R = 125$ as compared to $\sigma_{\mathrm{TS}}(\alpha = 1.885, R = 125) = -0.18$ for the plane channel.

For Reynolds numbers greater than $R = R_c \approx 150$ the base-geometry eddy-promoter steady flow becomes unstable, bifurcating to a time-periodic flow of frequency $\Omega_n \approx \Omega$. To investigate these supercritical states equations (1)–(7) are integrated to times sufficiently large that the effect of initial conditions has

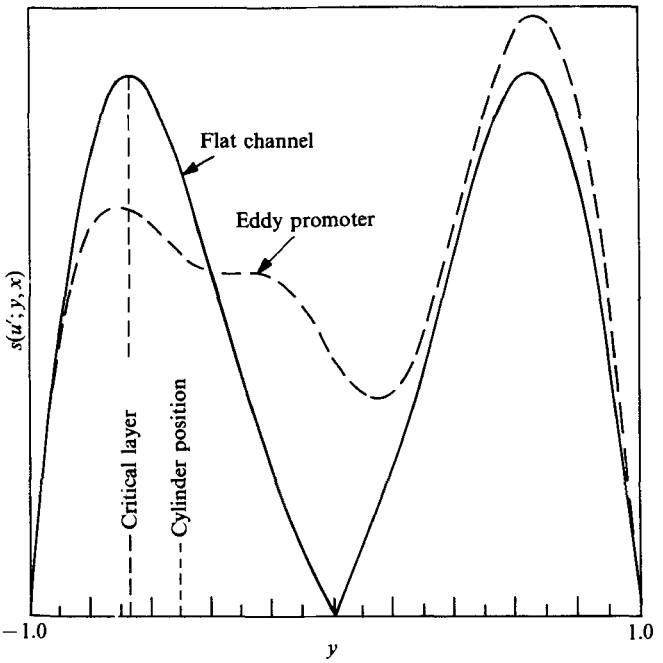

FIGURE 7. A comparison of the mode shape of the base-geometry eddy-promoter stability mode with that of the associated Orr–Sommerfeld flat-channel stability mode at $R = 125$. Except in the vicinity of the cylinder, the two mode shapes are quite similar, in particular as regards the location and structure of the critical layer.

disappeared, and only the steady-periodic solution remains. We plot in figure 8 the unsteady streamlines of a nonlinear steady-periodic secondary flow at $R = 225$ at several times during the flow cycle, $0 < t < \Omega_n^{-1}$. This flow corresponds to nonlinear saturation of (unstable versions) of the linear waves shown in figure 5, and resembles qualitatively the finite-amplitude Tollmien–Schlichting waves seen in plane channels at much higher Reynolds numbers (Orszag & Patera 1983). The bifurcation to unsteady flow can be shown to be a regular Hopf bifurcation (Karniadakis 1987).

Thus, in summary, the modes of eddy-promoter channel flow correspond to shear-layer destabilization of 'native' Tollmien–Schlichting waves, with the frequency of the plane-channel waves only slightly modified, but with their stability drastically altered. The fact that the critical Reynolds number of a flow can be reduced from $R_{c,TS} = 5772$ (for plane channels) to $R_c = 150$ (for eddy-promoter channels) without the form or frequency of the instability modes being substantially modified can be understood in terms of the relative magnitudes of the relevant quantities. In particular, if we assume that ϵ_d is some small parameter that measures the geometric and dynamic effect of the cylinder, we would expect that

$$\boldsymbol{v}_s = (1-y^2)\,\hat{\boldsymbol{x}} + O(\epsilon_d), \qquad \hat{\boldsymbol{v}}' = \hat{\boldsymbol{v}}'_{TS} + O(\epsilon_d), \tag{23a,b}$$

$$\Omega = \Omega_{TS} + O(\epsilon_d), \qquad \sigma = \sigma_{TS} + O(\epsilon_d), \tag{23c,d}$$

where all quantities on the left-hand side of (23) refer to the eddy-promoter flow.

Now, as both the eigenfunction and frequency of the plane-channel Tollmien–Schlichting waves are 'order one' quantities at these Reynolds numbers, we

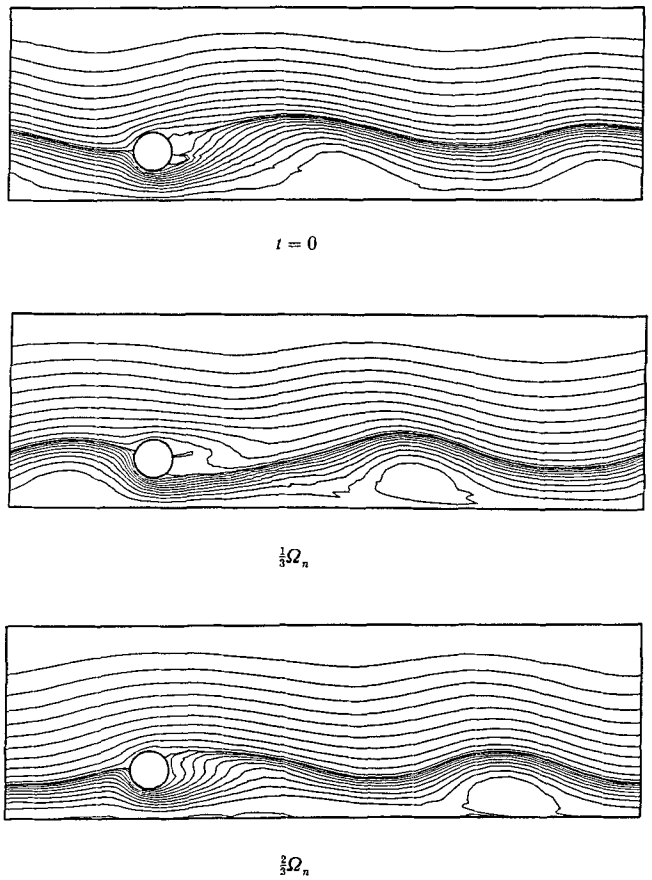

FIGURE 8. Streamlines of the supercritical eddy-promotor channel flow in the base geometry at $R = 225$ plotted at several times during the flow cycle $0 < t < \Omega_n^{-1}$. Ths steady-periodic flow corresponds to nonlinear saturation of unstable Tollmien–Schlichting-like travelling waves.

expect from (23*a–c*) that these aspects of the plane-channel modes will persist in the presence of small cylinders for which $\epsilon_d \ll 1$. On the other hand, as the growth rates of Tollmien–Schlichting waves are viscously small, $|\sigma_{TS}| \ll 1$, it is plausible that even a small cylinder can have a significant effect on the stability of plane Poiseuille flow. More precisely, the inflexional profile in figure 4(*a*) suggests a positive $O(\epsilon_d)$ term in (23*d*), which can in turn easily balance a small, negative σ_{TS} so as to produce a net positive growth rate.

To demonstrate that the theory described in the preceding paragraphs is generally valid for small-cylinder eddy-promoter flows, we have calculated the linear stability characteristics of a relatively large number of different geometries at $R = 125$. This Reynolds number is subcritical for all of the geometries investigated. For each geometry the steady solution is calculated, and the time-asymptotic solution of the linearized Navier–Stokes equations is then used to infer the frequency Ω, growth rate σ, and wavenumber $\alpha = 2\pi n/L$ of the solution, where n denotes the number of waves per periodicity length. For example, figures 9(*a*), 9(*b*), and 9(*c*) show the instantaneous streamlines of the stability calculations for $L = 6.66$, $d = 0.25$, $b = 0.5$; $L = 6.66$, $d = 0.25$, $b = 0.75$; and $L = 6.66$, $d = 0.25$, $b = 1.0$, for which $\Omega = 0.185$, $n = 2$; $\Omega = 0.357$, $n = 3$; and $\Omega = 0.476$, $n = 4$, respectively.

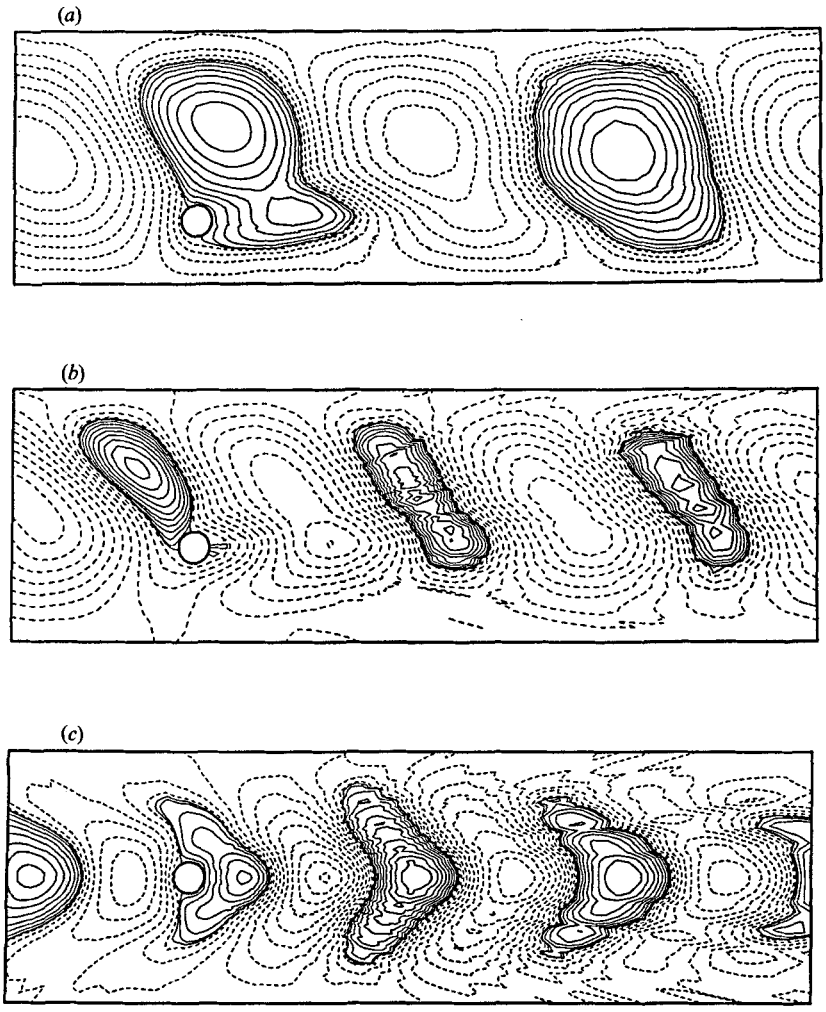

FIGURE 9. Instantaneous streamlines of the least-stable eddy-promoter-channel modes at $R = 125$ for (*a*) $L = 6.666$, $d = 0.25$, $b = 0.5$; (*b*) $L = 6.66$, $d = 0.25$, $b = 0.75$; and (*c*) $L = 6.666$, $d = 0.25$, $b = 1.0$. Cylinders near the wall excite low-wavenumber wall modes, whereas cylinders near the centre of the channel excite high-wavenumber centre modes.

In figure 10 we plot Ω as a function of α for the different eddy-promoter geometries listed in table 1. All the eddy-promoter frequencies are seen to lie on the flat-channel Orr–Sommerfeld dispersion relation to within a few percent, not dissimilar to the result obtained previously for grooved-channel flows. Indeed, the stability theory described here is generally valid for a wide class of flows corresponding to finite but small geometric perturbations of classical homogeneous-geometry internal flows (e.g. channels and pipes).

We shall now make several remarks concerning figure 10. First, the calculations are all performed with $m = 1$, corresponding to the assumption of 'strong' periodicity. Numerical calculations with $m = 2$ for the base geometry ($L = 6.66$, $d = 0.4$, $b = 0.5$) produce identical results to the corresponding calculations with $m = 1$ for both linear and nonlinear flows, indicating that this particular flow is, indeed, stable with respect to subharmonic disturbances. As d and L become small we no

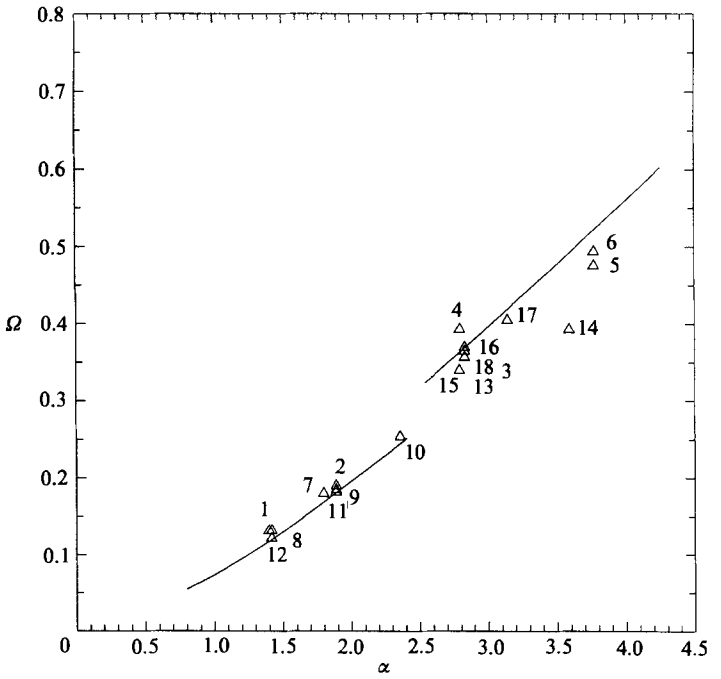

FIGURE 10. A plot of eddy-promoter frequency Ω ($\triangle_i$) as a function of wavenumber α at a Reynolds number of $R = 125$; the geometric parameters defining the different cases studied, i, are summarized in table 1. The solid line indicates the corresponding flat-channel least-stable-mode Orr–Sommerfeld relation. With the exception of the $L = 3.5$, $d = 0.4$, $b = 1.0$ geometry ($\triangle_{14}$), for which the effect of the cylinder is large due to the relatively small value of L, the eddy-promoter and flat-channel flows have remarkably similar dispersion relations.

Geometry	L	d	b	Ω	n
1	4.50	0.25	0.50	0.129	1
2	6.66	0.25	0.50	0.190	2
3	6.66	0.25	0.75	0.357	3
4	4.50	0.25	1.0	0.393	2
5	6.66	0.25	1.0	0.476	4
6	10.0	0.25	1.0	0.494	6
7	3.50	0.40	0.50	0.180	1
8	4.44	0.40	0.50	0.132	1
9	6.66	0.40	0.50	0.185	2
10	8.0	0.40	0.50	0.254	3
11	10.0	0.40	0.50	0.182	3
12	13.32	0.40	0.50	0.122	3
13	6.66	0.40	0.75	0.357	3
14	3.50	0.40	1.0	0.393	2
15	4.50	0.40	1.0	0.340	2
16	6.66	0.40	1.0	0.370	3
17	10.0	0.40	1.0	0.405	5
18	13.32	0.40	1.0	0.365	6

TABLE 1. The various geometries appearing in figure 10 ($\triangle_i$) in terms of periodicity length L, cylinder diameter d, and cylinder placement b. Also given is the frequency of the least-stable mode, and the number of waves per periodicity length, n ($\alpha = 2\pi n/L$). Note that all calculations are performed for $m = 1$; however, only for certain geometries (e.g. the base geometry with $L = 6.666$, $d = 0.4$, $b = 0.5$) has the validity of this assumption been verified.

longer expect $m = 1$ to be a reasonable assumption; for instance, for $L = 4.44$, $d = 0.4$, $b = 0.5$ we find that with $m = 2$ we obtain an $n = 3$ solution, whereas with $m = 1$ we obtain an $n = 1$ solution. In these cases the larger computational domain must be used.

Second, we note that at this Reynolds number the least-stable mode of the Orr–Sommerfeld operator changes from a wall mode to a centre mode at $\alpha \approx 2.50$, as reflected in the discontinuity in the dispersion relation in figure 10. Although our theory only predicts that $\Omega = \Omega_{\mathrm{TS}}(\alpha, R)$, and does not predict the spatial scale α that will be selected by the flow, it appears generally true that cylinders near the wall generate low wavenumbers associated with wall modes (see figure 9*a*), whereas cylinders near the centre of the channel generate high wavenumbers associated with centre modes (see figure 9*b*, *c*). This selection rule is consistent with the fact that the location of the critical layer of the excited Orr–Sommerfeld mode should be correlated with the position of the cylinder and associated inflexion points. It is thus clear that although the cylinders do not play a role in the dispersion relation, they do play a role in frequency selection.

Lastly, it is important to consider what role, if any, the mechanism of unbounded-flow isolated-cylinder vortex shedding plays in the frequency determination process in eddy-promoter channels. For the cases in which the cylinder is close to the wall and low-wavenumber modes are selected, it is clear that the instability-mode spatial structures (see figures 5–7 and 9*a*) are unambiguously inconsistent with the von Kármán vortex street (Gerard 1978). However, for eddy-promoter flows in which the cylinder is placed near the centre of the channel, as in figure 9(*c*), the wavenumber and frequency of the stability modes are no longer inconsistent with those of the infinite-domain cylinder wake. Nevertheless, the dominant stability structures even in this case still derive from the vortical background plane Poiseuille flow.

This is demonstrated in figure 11 by a comparison of mode shape $s(u'; y, x)$ for the eddy-promoter stability mode ($R = 150$, $L = 6.666$, $d = 0.4$, $b = 1$) and the least-stable Orr–Sommerfeld mode at the same Reynolds number and wavenumber ($\alpha = 2.83$). As for the near-wall modes (see figures 5–7), the eddy-promoter-channel structures are quite similar to their plane-channel-flow counterparts. The determining factor in deciding whether a Tollmien–Schlichting mechanism or a vortex-street mechanism will be operative in a particular flow is the background vorticity field in which the instability evolves; for a blunt irrotational incoming flow field (i.e. as in a non-fully developed laminar flow or a mean turbulent flow) the von Kármán vortex street will result, whereas for a parabolic background flow a Tollmien–Schlichting wave will be selected (G. E. Karniadakis, H. Kozlu & A. T. Patera, research in progress). This separation of mechanism has not been completely appreciated in the past (e.g. Shina, Takizuka & Okamoto 1977).

There are many important aspects of eddy-promoter stability theory related to inviscid–viscous analysis, single-cylinder non-periodic flow, supercritical behaviour, and three-dimensional secondary instability that we shall not consider here. In particular, it is important to determine if the viscous mean flows induced by eddy promoters (e.g. figure 3) are inviscidly unstable, or whether they still require the Tollmien–Schlichting viscous mechanism to achieve positive growth rates. Although these issues are of interest in their own right, they are not directly related to the transport enhancement-stability theory which is the central focus of the current paper. We thus relegate these topics to other publications (Karniadakis & Amon 1987; Amon & Patera 1988; G. E. Karniadakis, H. Kozlu & A. T. Patera, research in progress), and proceed directly to the consideration of dissipation-transport in supercritical eddy-promoter flows.

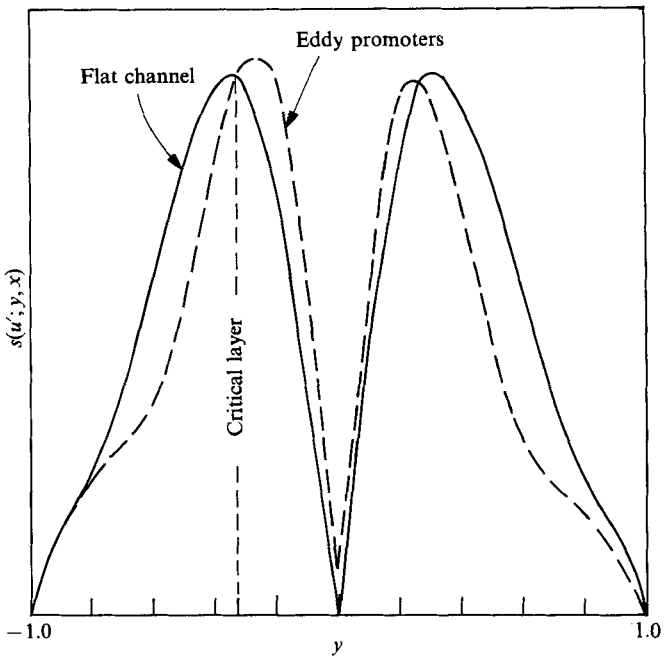

FIGURE 11. A comparison of the mode shape of the $L = 6.666$, $d = 0.4$, $b = 1.0$ (centred cylinder) eddy-promoter stability mode with that of the associated Orr–Sommerfeld flat-channel centre mode. As for the wall modes in figure 7, the agreement between the eddy-promoter and flat-channel centre-mode shapes is very good. Note the distinct wall and critical layers.

5. Dissipation transport in eddy-promoter flows

The Reynolds-analogy dissipation-transport theory presented in §3 suggests that if an eddy-promoter flow I can be created that is significantly more unstable than some other eddy-promoter (or flat-channel) flow II, then flow I will incur significantly less dissipation for a given heat transfer rate than flow II if the direct dissipation due to the cylindrical eddy promoter, Φ_C, can be maintained small. The stability theory presented in §4 indicates that small cylinders can drastically reduce the stability of channel flow, implying that destabilization and control of Φ_C are not physically inconsistent objectives. We now show that, indeed, very low-dissipation transport systems can be achieved using low-Reynolds-number supercritical eddy-promoter flows.

We begin by plotting in figure 12 the Nusselt number Nu as a function of Reynolds number R for the base geometry $L = 6.666$, $d = 0.4$, $b = 0.5$ (all results are for $Pr = 1.0$). For Reynolds numbers less than $R_c = 150$ the Nusselt number is in fact slightly less than that for plane-channel laminar flow, $Nu_0 = 1.35$. This is because the conduction penalty associated with the adiabatic cylinder outweighs the convective effect of the extremely weak, essentially parallel wake flow (see figure 3). However, for $R > R_c$ the Nusselt number increases dramatically owing to the Reynolds flux generated by the unsteady motion. Figure 12 serves as confirmation of our hypothesis that an unstable flow will lead to larger Nusselt numbers at lower Reynolds numbers.

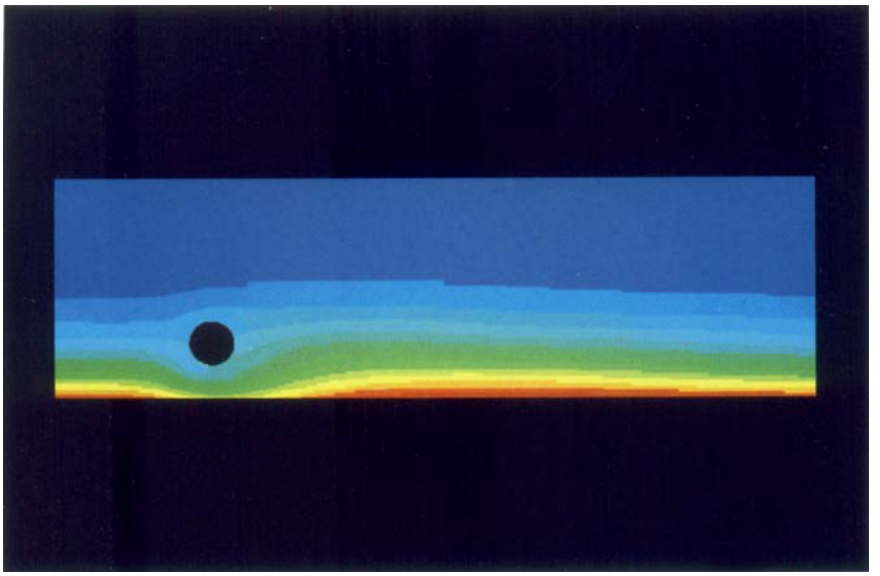

FIGURE 13. A plot of the isotherms of the steady subcritical flow for the base geometry at $R = 125$ (see figure 3 for the corresponding streamlines). The temperature is represented by the colour spectrum, with red (blue) corresponding to hot (cold). The temperature distribution differs only slightly from that for fully developed parallel flow in a flat channel.

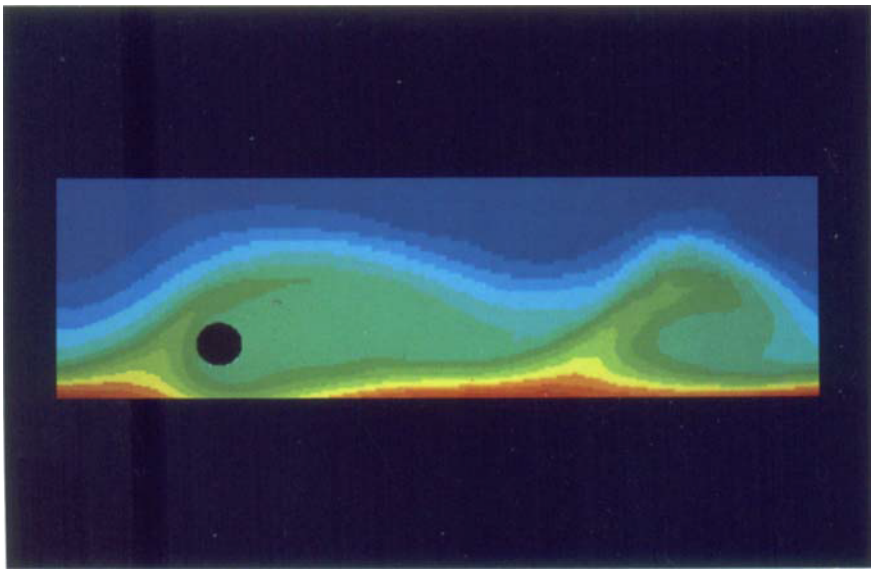

FIGURE 14. A plot of the unsteady isotherms at one instant in time of the steady-periodic supercritical flow for the base geometry at $R = 300$. Transport enhancement is effected by Tollmien–Schlichting-induced convective mixing. The similarity of the isotherms depicted here with those for grooved-channel flow (figure 18 of Ghaddar *et al.* 1986*c*) is indicative of the ubiquitous nature of Tollmien–Schlichting waves in internal flows.

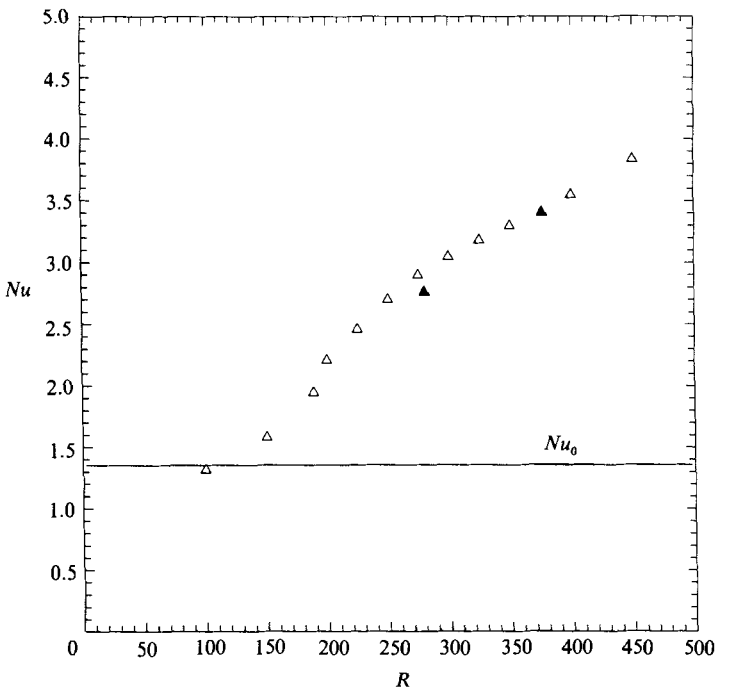

FIGURE 12. A plot of the Nusselt number for the base geometry $L = 6.666$, $d = 0.4$, $b = 0.5$ with $Pr = 1.0$: △, numerical; ▲, experimental (Kozlu *et al.* 1988). (The experimental data are obtained for air and scaled to $Pr = 1$ using the $Pr^{-\frac{1}{3}}$ scaling discussed in §3.2.) For $R > R_c$ the Nusselt number increases rapidly owing to the highly unsteady motion and associated large Reynolds flux. For $R > 500$ a three-dimensional secondary instability (Orszag & Patera 1983; Amon & Patera 1988) sets in that results in a discrepancy between the experimental and (assumed two-dimensional) numerical predictions.

To graphically illustrate the physical mechanism responsible for the increase in Nusselt number shown in figure 12, we plot in figure 13 (Plate 1) the steady isotherms at $R = 125$, and in figure 14 (Plate 1) the unsteady isotherms associated with a supercritical steady-periodic flow at $R = 300$. As for the case of resonantly forced subcritical grooved-channel flows (Ghaddar *et al.* 1986*c*), heat transport enhancement in supercritical eddy-promoter flows is due to strongly non-parallel finite-amplitude Tollmien–Schlichting waves which act as effective heat exchangers between the heated wall and the bulk fluid.

Figure 14 also demonstrates two critical facts germane to the validity of the Reynolds analogy. First, the strong wavy nature of the flow indicates that the heat transfer is effected via Reynolds' fluxes and convective–diffusive balance rather than through (mean) molecular gradient diffusion. This is illustrated more quantitatively in figure 15 as a plot of the Reynolds flux,

$$\mathscr{F}(y;x) = R\,Pr\langle v'\theta'\rangle = R\,Pr\,\Omega_n \int_t^{t+1/\Omega_n} [v'(\boldsymbol{x},t')\,\theta'(\boldsymbol{x},t')]\,\mathrm{d}t', \tag{24}$$

at $x = 6.5$ and $R = 450$. Here v' and θ' are the fluctuating components of vertical velocity and temperature, $v' = v - \langle v\rangle$ and $\theta' = \theta - \langle\theta\rangle$, respectively. The fact that

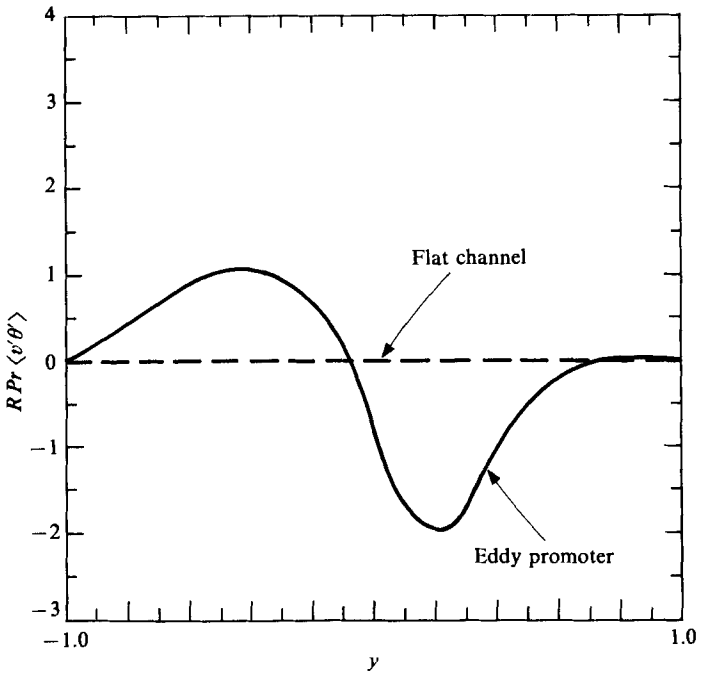

FIGURE 15. A plot of the Reynolds flux $RPr\langle v'\theta'\rangle$ at $x = 6.5$ and $R = 450$ in the base geometry $L = 6.66$, $d = 0.40$, $b = 0.5$. The order-unity Reynolds flux demonstrates the importance of convective transport in supercritical eddy-promoter flows.

$\mathscr{F}$ is order unity demonstrates that the majority of the heat in the interior is transferred via fluctuations rather than through molecular diffusion through the mean gradient.

Second, it can be seen in figure 14 that the structure responsible for heat transfer is the spatially homogeneous Tollmien–Schlichting wave, not the local boundary-layer effects in the vicinity of the cylinder. We demonstrate this feature more quantitatively by plotting in figure 16 $\langle\theta(x, y = -1)\rangle^{-1}$ (a local Nusselt number) along the bottom wall, $0 < x < L$, for $R = 225$ and the base geometry. The most significant increase in the space-averaged Nusselt number is clearly due to the overall shift of level compared to the subcritical flow, not due to the local flow deflection caused by the cylinder.

Given the convective–diffusive balance and wall structure 'universality' demonstrated in figures 14–16 we expect the Reynolds analogy to be valid in supercritical eddy-promoter flows. We verify this by plotting in figure 17 the Reynolds-analogy constant γ as a function of Reynolds number R. (Note γ is calculated from (19) based on the numerical data for the total dissipation Φ, the Nusselt number Nu, and the cylinder drag.) As expected, once the Reynolds number is slightly greater than R_c, γ rapidly approaches unity. It is clear from figure 17 that the Reynolds analogy is equally valid for laminar and turbulent flows as long as sufficient mixing takes place (measured, for instance, by $(Nu\text{-}Nu_0)/Nu_0$).

The last piece of the dissipation-transport equation is the non-analogous loss arising from direct dissipation due to the eddy promoters. In particular, if the non-analogous losses are not to dominate the analogous components of momentum

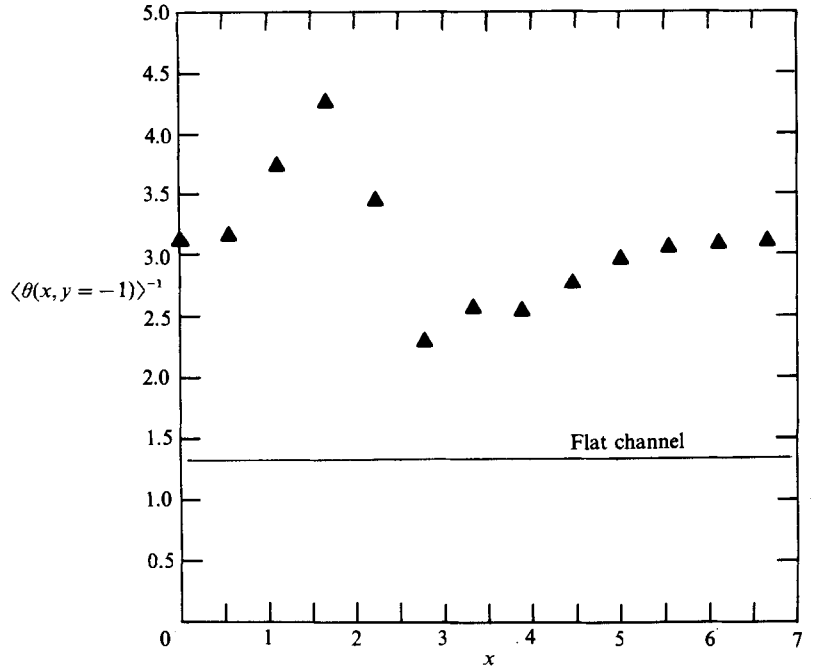

FIGURE 16. A plot of the local time-averaged Nusselt number $\langle\theta\rangle^{-1}$ along the bottom wall $0 < x < L$, for $R = 225$ in the base geometry. The most significant increase in heat transfer over the subcritical case ($\langle\theta\rangle^{-1} \approx 1.35$) is due to the spatially homogeneous Tollmien–Schlichting wave, not due to the local flow phenomena induced by the cylinder.

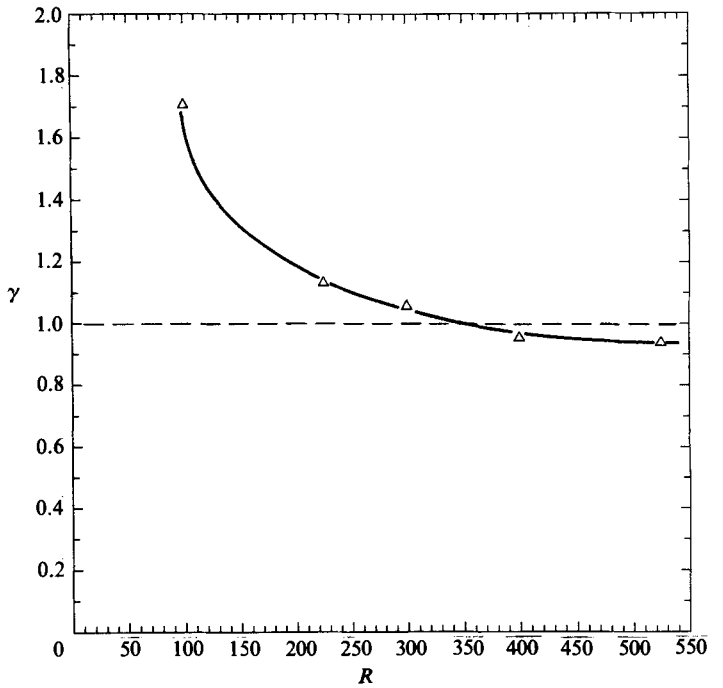

FIGURE 17. A plot of the Reynolds-analogy constant γ as a function of Reynolds number. For $R > R_c$ the analogy constant approaches unity, reflecting the presence of a strongly convective–diffusive transport mechanism.

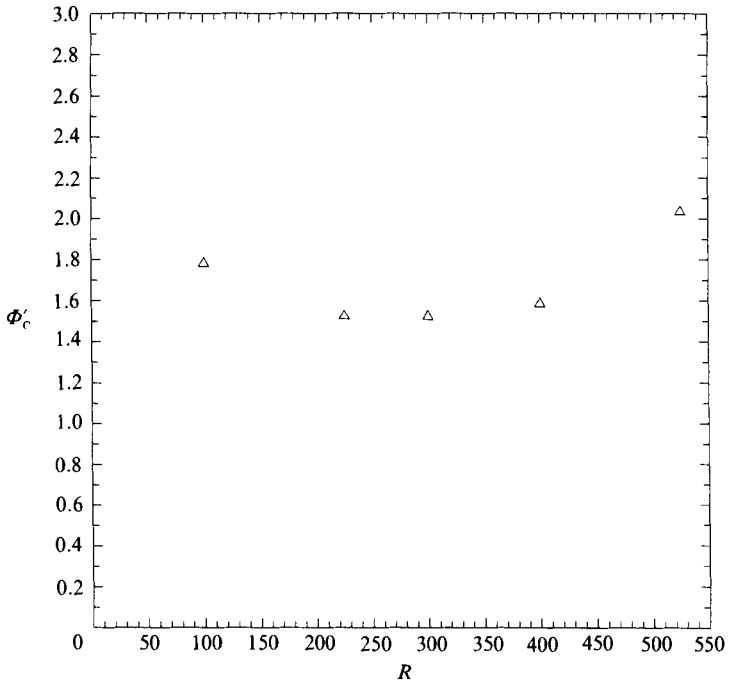

FIGURE 18. A plot of the non-analogous dissipation Φ'_C as a function of Reynolds number. The non-analogous dissipation is order unity; however, it grows with increasing R owing to the fact that the Nusselt number grows slower than linearly with Reynolds number.

transport in (19a), we must have that $\Phi'_C = 3\Phi_C/R^2Nu$ is order unity or less, where from (19b)

$$\Phi'_C = \left\{\frac{1}{6}\left(\frac{d}{L}\right)\left(\frac{V_C}{V}\right)^2\right\} C_D \frac{R}{Nu}. \tag{25}$$

The geometric terms in brackets in (25) will be $O(d/L) \ll 1$, and thus if C_D and R/Nu are not too large, the entire quantity will be small. Our numerical results indicate that C_D is quite close to its (pre-drag-crisis) large-R asymptotic value for unbounded flow past an isolated cylinder, $C_D = 1.30$ (Tritton 1959; Karniadakis 1988). As for our flows R/Nu is on the order of 100, it follows that Φ'_C is order unity. This is shown to be the case in figure 18, which is a plot of Φ'_C as a function of Reynolds number. Note the non-analogous dissipation grows for larger R because the Nusselt number grows slower than linearly with Reynolds number.

We conclude that eddy-promoter flows achieve significant heat transfer at low Reynolds number, and do so while roughly preserving the Reynolds analogy ($\gamma \sim 1$, Φ'_C not large). This directly implies reduction in dissipation from the theory of §3.3; we demonstrate this result in figure 19 as a plot of dissipation Φ as a function of Nusselt number Nu. In addition to the base-geometry eddy-promoter data we have also plotted results for transitional and low-Reynolds-number turbulent flat-channel ($d = 0$) flows (H. Kozlu, research in progress), from which it is seen that the eddy-promoter flows can save up to 500% in dissipation in the Nusselt-number range plotted. The qualitative features of the dissipation-transport relation shown in figure 19 appear to be generally valid, even in more complicated configurations than the periodic eddy-promoter geometry studied here.

At larger Reynolds numbers the dissipation reduction in eddy-promoter flows

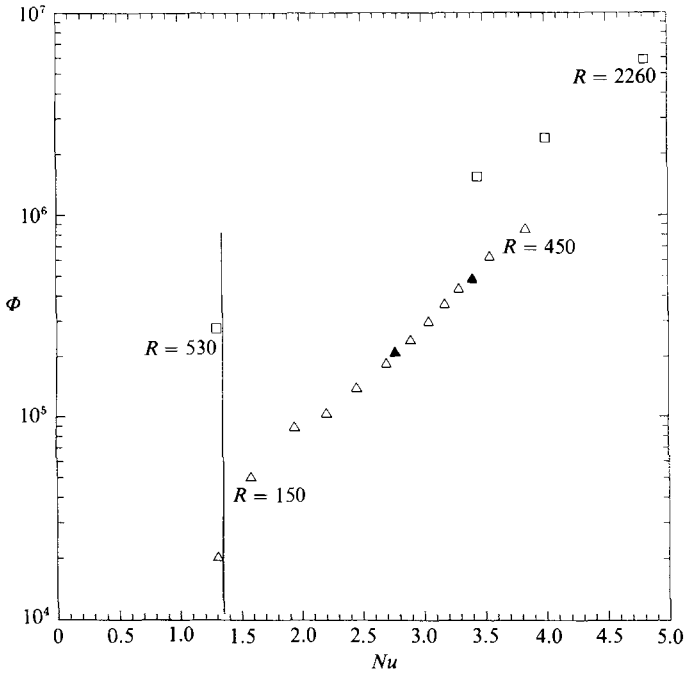

FIGURE 19. A plot of dissipation as a function of Nusselt number for the base-geometry eddy-promoter flow: △, numerical; ▲, experimental (Kozlu *et al.* 1988). Also shown is the solution for laminar flat-channel ($d = 0$) flow (solid line), and data for transitional and low-Reynolds-number turbulent flat-channel ($d = 0$) flow (□) (H. Kozlu, research in progress). Flow destabilization results in significant savings in dissipation.

decreases owing to growth of Φ'_C through increases in R/Nu. This trend continues in the turbulent flow regime, although there is an interesting exception at transition ($R \approx 800$) due to a premature drag crisis on the cylinder (Kozlu *et al.* 1988). The decrease in dissipation reduction at higher laminar and turbulent Reynolds numbers is due to nonlinear saturation, that is, the scales of motion destabilized by the eddy promoters are increasingly naturally unstable (e.g. the turbulent energy cascade). As a result, the eddy-promoters yield little increase in heat transfer, yet continue to contribute to dissipation via non-analogous cylinder drag.

This result suggests that as the Reynolds number and Nusselt number increase, destabilization should be applied at the naturally stable scales of motion (such as the viscous sublayer in turbulent flow (Kozlu *et al.* 1988)) if significant reduction in dissipation is to be realized. Study of transport enhancement by scale-matched flow destabilization is the natural extension of the present investigation, and is currently underway.

We would like to thank Professor Ain A. Sonin for helpful discussions. We would also like to acknowledge Mr Hamdi Kozlu for his contributions to this paper, and for making his experimental data available prior to publication. This work was supported by the National Science Foundation under Grant CBT 85-06146, and by the Office of Naval Research and the Defense Advanced Research Projects Agency under Contract N00014-85-K-0208. Some of the calculations were performed on the NASA-Ames CRAY X-MP.

REFERENCES

AMON, C. H. & PATERA, A. T. 1988 Numerical calculation of stable three-dimensional tertiary states in grooved-channel flow. *Phys. Fluids* (submitted).

BERGLES, A. E. & WEBB, R. L. 1985 A guide to the literature on convective heat transfer augmentation. *Advances in Enhanced Heat Transfer, 23rd Natl Heat Transfer Conf. Denver.*

DRAZIN, P. G. & REID, W. H. 1981 *Hydrodynamic Stability.* Cambridge University Press.

GERARD, J. H. 1978 The wakes of cylindrical bluff bodies at low Reynolds number. *Proc. R. Soc. Lond.* A **289**, 351.

GHADDAR, N. K., KARNIADAKIS, G. E. & PATERA, A. T. 1986*a* A conservative isoparametric spectral element method for forced convection; application to fully developed flow in periodic geometries. *Numer. Heat Transfer* **9**, 277.

GHADDAR, N. K., KORCZAK, K. Z., MIKIC, B. B. & PATERA, A. T. 1986*b* Numerical investigation of incompressible flow in grooved channels. Part 1. Stability and self-sustained oscillations. *J. Fluid Mech.* **163**, 99.

GHADDAR, N. K., MAGEN, M., MIKIC, B. B. & PATERA, A. T. 1986*c* Numerical investigation of incompressible flow in grooved channels. Part 2. Resonance and oscillatory heat transfer enhancement. *J. Fluid Mech.* **168**, 541.

GIRAULT, V. & RAVIART, P. A. 1986 *Finite Element Approximation of the Navier–Stokes Equations.* Springer.

GOTTLIEB, D. & ORSZAG, S. A. 1977 *Numerical Analysis of Spectral Methods.* SIAM.

HERBERT, T. 1976 Periodic secondary motions in a plane channel. In *Proc. 5th Intl Conf. on Numerical Methods in Fluid Dynamics* (ed. A. I. van de Vooren & P. J. Zandbergen), Lecture notes in Physics, vol. 59, p. 235. Springer.

ISAACSON, M. S. & SONIN, A. A. 1976 Sherwood number and friction factor correlations for electrodialysis systems, with application to process optimization. *I & EC Process Des. Dev.* **15**, 313.

KARNIADAKIS, G. E. 1987 The spectral element method applied to heat transport enhancement by flow destabilization. Ph.D. thesis, M.I.T.

KARNIADAKIS, G. E. 1988 Numerical simulation of heat transfer from a cylinder in crossflow. *Intl J. Heat Mass Transfer* (to appear).

KARNIADAKIS, G. E. & AMON, C. H. 1987 Stability calculations of wall bounded flows in complex geometries. In *Proc. Sixth IMACS Intl Symp. on Comp. Meth. for Partial Differential Equations*, p. 525.

KAYS, W. M. & CRAWFORD, M. E. 1980 *Convective Heat and Mass Transfer.* McGraw-Hill.

KORCZAK, K. Z. & PATERA, A. T. 1986 An isoparametric spectral element method for solution of the Navier–Stokes equations in complex geometry. *J. Comp. Phys.* **62**, 361.

KOZLU, H. 1988 Experimental investigation of heat removal from a surface, PhD thesis, MIT (in progress).

KOZLU, H., MIKIC, B. B. & PATERA, A. T. 1988 Minimum-dissipation heat removal by scale-matched flow destabilization. *Intl J. Heat Mass Transfer* (to appear).

MADAY, Y. & PATERA, A. T. 1988 Spectral element methods for the incompressible Navier–Stokes equations. In *State of the Art Surveys in Computational Mechanics* (ed. A. K. Noor), ASME (to appear).

MAGEN, M., MIKIC, B. B. & PATERA, A. T. 1988 Bounds for conduction and forced convection heat transfer. *Intl J. Heat Mass Transfer* (to appear).

MIKIC, B. B. 1981 A model for turbulent transport near a wall. In *Proc. Congr. for Theoretical and Applied Mechanics*, Kupari, Yugoslavia, p. 119.

ORSZAG, S. A. 1971 Accurate solution of the Orr–Sommerfeld stability equation. *J. Fluid Mech.* **50**, 689.

ORSZAG, S. A. & PATERA, A. T. 1983 Secondary instability of wall-bounded shear flows. *J. Fluid Mech.* **128**, 347.

PATANKAR, S. V., LIU, C. H. & SPARROW, E. M. 1977 Fully developed flow and heat transfer in ducts having streamwise-periodic variations of cross-sectional area. *J. Heat Transfer* **99**, 180.

PATERA, A. T. 1984 A spectral element method for fluid dynamics: laminar flow in a channel expansion. *J. Comp. Phys.* **54**, 468.

REYNOLDS, O. 1874 On the extent and action of the heating surface for steam boilers. *Proc. Manchester Lit. Phil. Soc.* **14**, 7.

RØNQUIST, E. M. & PATERA, A. T. 1987 A Legendre spectral element method for the Stefan problem. *Intl J. Num. Meth. Engng* **24**, 2273.

SCHLICHTING, H. 1968 *Boundary Layer Theory*, 6th edn. McGraw-Hill.

SHINA, Y., TAKIZUKA, T. & OKAMOTO, Y. 1977 Flow visualization around turbulence promoters in parallel, convergent and divergent channels. In *Proc. Intl Symp. on Flow Visualization, Tokyo, Japan,* p. 149.

TAYLOR, G. I. 1930 The application of Osborne Reynolds's theory of heat transfer to flow through a pipe. *Proc. R. Soc.* A, ***CXXIX***, 25.

THOMAS, L. C. 1979 Turbulent burst phenomenon. In *Turbulent Forced Convection in Channels and Bundles*, vol. 1, p. 491. Hemisphere.

TRITTON, D. J. 1959 Experiments on the flow past a circular cylinder at low Reynolds numbers. *J. Fluid Mech.* **6**, 547.